Silicon oxynitride films deposited by reactive high power impulse magnetron sputtering using nitrous oxide as a single-source precursor

Tuomas Hänninen, Susann Schmidt, Jens Jensen, Lars Hultman and Hans Högberg

Original Publication:

Tuomas Hänninen, Susann Schmidt, Jens Jensen, Lars Hultman and Hans Högberg, Silicon oxynitride films deposited by reactive high power impulse magnetron sputtering using nitrous oxide as a single-source precursor, 2015, Journal of Vacuum Science & Technology. A. Vacuum, Surfaces, and Films, (33), 5, 05E121.
http://dx.doi.org/10.1116/1.4927493

JVSTA Journal of Vacuum Science & Technology A

Silicon oxynitride films deposited by reactive high power impulse magnetron sputtering using nitrous oxide as a single-source precursor

Tuomas Hänninen, Susann Schmidt, Jens Jensen, Lars Hultman, and Hans Högberg

Citation: Journal of Vacuum Science & Technology A **33**, 05E121 (2015); doi: 10.1116/1.4927493
View online: http://dx.doi.org/10.1116/1.4927493
View Table of Contents: http://scitation.aip.org/content/avs/journal/jvsta/33/5?ver=pdfcov
Published by the AVS: Science & Technology of Materials, Interfaces, and Processing

Silicon oxynitride films deposited by reactive high power impulse magnetron sputtering using nitrous oxide as a single-source precursor

Tuomas Hänninen,[a] Susann Schmidt, Jens Jensen, Lars Hultman, and Hans Högberg
Thin Film Physics Division, Department of Physics, Chemistry, and Biology (IFM), Linköping University, Linköping SE-581 83, Sweden

(Received 17 May 2015; accepted 13 July 2015; published 29 July 2015)

Silicon oxynitride thin films were synthesized by reactive high power impulse magnetron sputtering of silicon in argon/nitrous oxide plasmas. Nitrous oxide was employed as a single-source precursor supplying oxygen and nitrogen for the film growth. The films were characterized by elastic recoil detection analysis, x-ray photoelectron spectroscopy, x-ray diffraction, x-ray reflectivity, scanning electron microscopy, and spectroscopic ellipsometry. Results show that the films are silicon rich, amorphous, and exhibit a random chemical bonding structure. The optical properties with the refractive index and the extinction coefficient correlate with the film elemental composition, showing decreasing values with increasing film oxygen and nitrogen content. The total percentage of oxygen and nitrogen in the films is controlled by adjusting the gas flow ratio in the deposition processes. Furthermore, it is shown that the film oxygen-to-nitrogen ratio can be tailored by the high power impulse magnetron sputtering-specific parameters pulse frequency and energy per pulse. [http://dx.doi.org/10.1116/1.4927493]

I. INTRODUCTION

Silicon oxynitride has received considerable interest during the past years, given its diversity of useful material properties.[1–8] One of the beneficial aspects of silicon oxynitride (SiO_xN_y) thin films is the possibility to tailor the properties by adjusting the relative amounts of oxygen and nitrogen in the material. This yields properties ranging from and beyond those of amorphous silicon (a-Si), silicon nitride, and silicon oxide, or a mixture thereof. These possibilities are especially useful in optoelectronics, where SiO_xN_y has applications in graded refractive index layers,[5,9] antireflection coatings,[2] and optical waveguides.[10,11] Various deposition methods have been used to grow SiO_xN_y films by varying oxygen to nitrogen ratios. These include chemical vapor deposition (CVD),[4,5,7] laser ablation,[9,12] plasma nitridation,[13,14] and magnetron sputtering.[3,6] The use of CVD methods is limited due to hydrogen-containing precursors, as hydrogen has a deteriorating effect on the optical properties of SiO_xN_y thin films through the formation of N–H bonds.[10,11] Conventionally two reactive gases, O_2 and N_2, have been used to supply each element when SiO_xN_y has been synthesized by reactive magnetron sputtering.[1,2] The two-gas approach is challenging as accurate control of both reactive gas flows is difficult due to nonlinear target effects as a function of the reactive gas flow rate.[15] A reactive gas pulsing process can be used to overcome these nonlinear effects, but requires additional instrumentation to control the pulsing of the reactive gas.[16,17]

In order to tailor the reactive deposition process further, we chose reactive high power impulse magnetron sputtering (rHiPIMS) as the deposition method. High power impulse magnetron sputtering (HiPIMS) is an ionized physical vapor deposition technique based on conventional direct current magnetron sputtering.[18,19] In HiPIMS, short high voltage pulses are delivered to the cathode, resulting in highly ionized and dense plasmas for target metals.[19] The high degree of ionization of the sputtered material has been shown to improve the density of the grown films along with their morphology.[20–22] HiPIMS also offers a possibility to affect the film properties by adjusting the pulse-related deposition parameters, namely, the pulse frequency and energy per pulse.[19,23] Reduced or even eliminated hysteresis effects were also reported for HiPIMS.[24] Reactive HiPIMS has been demonstrated for various different thin film materials ranging from metal compounds to ceramics during the last decade.[25–32]

To eliminate the nonlinear effects of having two reactive gases, we employed nitrous oxide (N_2O) as a single-source precursor gas in the rHiPIMS deposition of SiO_xN_y. The behavior of nitrous oxide during the reactive sputter deposition was not yet investigated, but its effects on the plasma chemistry can be predicted by consideration of the ionization and dissociation pathways of the molecule.

Table I summarizes relevant data for the Si/Ar/N_2O discharge. As can be seen, the ionization energy of N_2O [$E_{P,N_2O} = 12.9$ eV (Ref. 35)] is lower than the ionization energy of Ar [$E_{P,Ar} = 15.8$ eV (Ref. 34)]. Upon electron impact, the N_2O molecule is either ionized or undergoes dissociative ionization along the following channels:

$$N_2O \xrightarrow{e^-} N_2O^+ + 2e^- \qquad E = 12.9\,\text{eV},$$
$$N_2O \xrightarrow{e^-} NO^+ + N + 2e^- \qquad E = 15.3\,\text{eV},$$
$$N_2O \xrightarrow{e^-} O^+ + N_2 + 2e^- \qquad E = 15.3\,\text{eV},$$
$$N_2O \xrightarrow{e^-} N_2^+ + O + 2e^- \qquad E = 17.3\,\text{eV},$$
$$N_2O \xrightarrow{e^-} N^+ + NO + 2e^- \qquad E = 20.3\,\text{eV}.$$

[a]Electronic mail: tuoha@ifm.liu.se

TABLE I. First ionization energies of Si, Ar, and N_2O plus total electron impact cross sections for Ar and N_2O.

	Species		
	Si	Ar	N_2O
First ionization energy (eV)	8.2 (Ref. 33)	15.8 (Ref. 34)	12.9 (Ref. 35)
Total cross section at 30 eV (10^{-18} cm^2)	—	175 (Ref. 36)	158 (Ref. 37)
Total cross section at 100 eV (10^{-18} cm^2)	—	270 (Ref. 36)	377 (Ref. 37)

As seen from the appearance energies of the N_2O dissociation products in Table II, the ionized fragments containing oxygen, like NO^+ and O^+, appear at lower energies than the nitrogen species N_2^+ and N^+. Additionally, the partial electron impact ionization cross sections presented in Table II imply that low electron energies favor the production of oxygen-containing species. Furthermore, the production of O^- ions through dissociative electron attachment has also been shown to contribute to the splitting of the N_2O molecule[40]

$$N_2O \xrightarrow{e^-} O^- + N_2.$$

These ions were shown to exhibit relatively long lifetimes during the discharge afterglow between the HiPIMS pulses.[41] The presence of O^- is observed already at zero electron energies at gas temperatures above the room temperature.[42] The reaction cross section increases with increasing gas temperature and values are of the same order of magnitude as the electron impact ionization cross sections for N_2O.[42] As can be understood from the dissociation scheme, the presence of multiple ion species and precursor fragments can be expected in the rHiPIMS plasma.

In this article, we investigate the effects of rHiPIMS process parameters on the resulting SiO_xN_y thin film properties. Furthermore, the effects of the reactive gas flow, pulse frequency, and energy per pulse on the chemical composition of the films and their chemical bonding structure are presented and discussed.

II. EXPERIMENTAL METHODS

All films were deposited with the industrial coating system CC800/9 (CemeCon AG, Germany).[43] In our experiments, one rectangular silicon target (area 440 cm^2) was sputtered in Ar/N_2O atmosphere keeping a constant deposition pressure of 400 mPa. The cathode was operated in power-regulated HiPIMS mode with a pulse width of 200 μs for all deposition processes. The substrates faced the target at a distance of 60 mm during the depositions. Moreover, a pulsed bias voltage (V_b) of −100 V, synchronized with the cathode pulse, was applied to the substrate table. Depositions were performed at a substrate temperature of 350 °C. The films were deposited on boron doped Si(100) substrates, using the above-mentioned settings. Three different deposition series were prepared; (1) variation of the percentage of nitrous oxide in the plasma, (2) variation of the pulse frequency, and (3) variation of the pulse energy.

For (1), the amount of N_2O in the working gas was varied by adjusting the flows of Ar and N_2O

$$f_{N_2O/Ar} = \frac{f_{N_2O}}{f_{Ar}} \times 100\,\%, \tag{1}$$

where f_{N_2O} is the flow of nitrous oxide and f_{Ar} is the flow of argon, respectively. The flow of N_2O was varied from 0 to 25 sccm, corresponding to $f_{N_2O/Ar}$ of 0% to 6.2%. Here, a pulse frequency of 600 Hz and an average cathode power of 2400 W, resulting in pulse energies of ∼4 J were used. For (2), different frequencies of 200, 400, 600, and 800 Hz were studied, using average cathode powers of 800, 1600, 2400, and 3200 W, respectively. The power was varied in order to maintain a pulse energy of ∼4 J. The reactive gas flow was kept at 10 sccm, corresponding to an $f_{N_2O/Ar}$ of 2.4%. For (3), the pulse energy was varied from 2 to 6 J in 1 J steps by changing the average target power from 1200 to 3600 W in 600 W steps, while the frequency was kept at 600 Hz. Here, an $f_{N_2O/Ar}$ of 2.4% was used. Target current and voltage waveforms during depositions were recorded with a Tektronix DPO4054 500 MHz bandwidth digital oscilloscope.

Cross-sectional scanning electron microscopy (SEM, LEO 1550 Gemini, Zeiss, Germany) was used to measure film thicknesses and to investigate the film morphology. To assess the structural properties of the films, x-ray diffraction (XRD) was carried out. A Philips powder diffractometer (PW 1820) equipped with a Cu(Kα) radiation source was operated at 40 kV and 40 mA, in order to record $\theta/2\theta$ scans. The residual film stresses were assessed by wafer curvature method, using XRD (PANalytical Empyrean) operated at 45 kV and 40 mA.[44] The Stoney formula for anisotropic single crystal Si(100) was applied to relate the measured substrate curvature to the residual thin film stress, assuming uniform plane stress in the film[45]

$$\sigma_f t_f = \frac{h^2 M^{Si}_{(100)}}{6R}, \tag{2}$$

TABLE II. Appearance energies and partial electron impact cross sections for N_2O fragments upon electron impact.

	Species				
	N_2O^+	NO^+	O^+	N_2^+	N^+
Appearance energy (eV)	12.9 (Ref. 35)	15.3 (Ref. 38)	15.3 (Ref. 39)	17.3 (Ref. 38)	20.3 (Ref. 39)
Partial cross section at 30 eV (10^{-18} cm^2) (Ref. 37)	102	34.4	4.66	14.1	2.37
Partial cross section at 100 eV (10^{-18} cm^2) (Ref. 37)	156	86.5	34.7	37.9	61.8

where σ_f is the in-plane stress component in the film, t_f is the film thickness, h is the substrate thickness, $M^{Si}_{(100)}$ is the biaxial modulus of Si(100) (180.3 GPa), and R is the radius of the curvature of the substrate. The same instrument was utilized to perform x-ray reflectivity (XRR) measurements. PANalytical X'Pert Reflectivity software was used to iteratively fit the measured XRR curves to evaluate the film density. A layered model containing the substrate, the film, and oxides both on the film and the substrate was assumed.

Time-of-flight elastic recoil detection analysis (ERDA) was carried out to obtain the elemental composition of the films.[46,47] A 36 MeV $^{127}I^{8+}$ ion beam with an incident angle of 22.5° relative to the sample surface was used. To study chemical bonding in the films, x-ray photoelectron spectroscopy (XPS, Axis Ultra^{DLD}, Kratos Analytical, Manchester, UK) with monochromatic Al(Kα) x-rays ($h\nu = 1486.6$ eV) was employed. The base pressure in the analysis chamber remained below 1×10^{-7} Pa during acquisition. Core level spectra of the Si 2p, N 1s, O 1s, Ar 2p, and C 1s regions were recorded on as-deposited samples and after a sputter clean of 120 s with 2 keV Ar^+ beam rastered over 3×3 mm^2 surface area at an incident angle of 70° with respect to the surface normal. Sputter cleaning resulted in a decreased resolution of the Si 2p core level spectra components, suggesting structural modification to the films due to the sputter ion impact. Therefore, the core level spectra acquired from the as-deposited samples were analyzed. Automatic charge compensation was used during the acquisition of all spectra. A Shirley-type background was subtracted from all spectra prior to peak fitting. Voigt peak shapes with the Lorentzian contribution of 30% were used to model the chemical structure of the SiO_xN_y films. In order to ensure a reliable peak fit model, Si 2p spectra were recorded for thermally grown silicon dioxide (SiO_2), CVD-grown silicon nitride (Si_3N_4), and pure Si deposited by comparable deposition parameters serving as internal references for the SiO_xN_y films. These reference samples were used to identify the number of components in the Si 2p region. All spectra were referenced to C–C bond, at 284.8 eV.[48]

Spectroscopic ellipsometry was used to study the optical constants of the films. The measurements were performed with a variable angle spectroscopic ellipsometer (J.A. Woollam Co.) at four incident angles 45°, 55°, 65°, and 75° over a wavelength range of 245–1690 nm. The data were analyzed with a COMPLETEEASE software version 4.72 and fitted with a Tauc–Lorentz model for amorphous films to assess their optical properties.[49]

III. RESULTS AND DISCUSSION

A. Process characteristics

Figure 1 shows a typical current and voltage waveform recorded during the rHiPIMS discharge of Si in Ar/N_2O plasmas. For the investigated range of processes, the target current and voltage waveforms did not change significantly with respect to their onset of rise, slope, and peak values. As shown in the inset of Fig. 1, increasing nitrous oxide flows during deposition results in slightly lower peak target currents, which is commonly ascribed to target poisoning.[50] However, within the range of studied reactive gas flows, the deposition rates did not change significantly, indicating that all processes were carried out in the metallic or transition region of the reactive discharge. Thus, the target was not poisoned and metallic target surface conditions can be assumed.[51] This suggests that the drop in the peak target current is mainly caused by a decreased secondary electron emission yield (γ_{SE}) as a consequence of increased N_2O flows.[52] The secondary electron emission yield was calculated according to the below equation:[53]

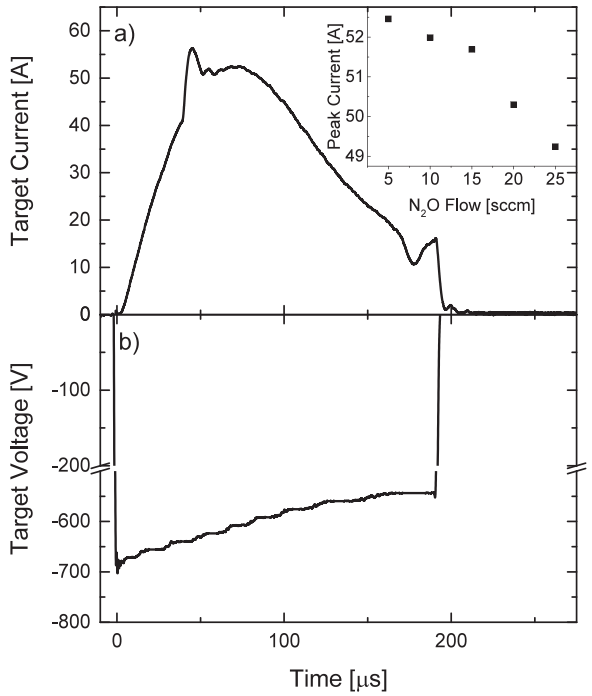

FIG. 1. Target current (a) and voltage (b) waveforms of the deposition process involving 5 sccm of nitrous oxide. The decrease of the peak target current vs increasing nitrous oxide flow is illustrated in the inset.

$$\gamma_{SE} = 0.032(0.78E_P - 2\phi), \tag{3}$$

where E_P is the first ionization energy of the arriving ion and ϕ is the work function of the target surface. When estimating γ_{SE} for Si discharges in N_2O and Ar using E_P values of 12.9 and 15.8 eV, respectively, and a value of 4.6 eV (Ref. 54) for the silicon target work function, the secondary electron yield by Ar^+ bombardment is approximately four times higher compared to the case when pure N_2O is used. Therefore, the drop of 3 A in peak target current can be ascribed to the increase in N_2O, as 25 sccm corresponding to a $f_{N_2O/Ar}$ of 6.2% is used. Moreover, the plasma density may be slightly reduced upon introduction of N_2O, due to its dissociation into precursor fragments and their further ionization. This may contribute to reduced peak target currents. However, considering the low N_2O ionization energy of 12.9 eV and comparing this to ionization and appearance energies of Ar^+ (cf. Table I) and possible N_2O precursor fragments (cf. Table II) in the plasma of >15 eV together with the rather high ionization cross section of N_2O (cf. Table I), we infer

that the direct ionization of the N_2O molecule is most probable. Hence, the effect of a reduced plasma density on the peak target current upon introduction of 25 sccm N_2O is considered to be minor. The decrease in target current is accompanied by an increase in the target voltage (not illustrated), since the processes were carried out in power-regulated mode. A decrease of the peak target current is not observed for depositions with varying pulse frequencies at an N_2O flow of 10 sccm, implying equal target surface chemistries and secondary electron yields for these processes. Raising the energy per pulse results in inherently increasing peak target currents and voltages. Here, the target voltage waveforms show an increasing voltage drop as the target current reaches its maximum. To conclude, an altered target surface or secondary electron yields cannot be drawn from these waveforms.

B. Thin film characterization

Cross-sectional SEM shows a dense and featureless morphology with a smooth surface structure for all investigated films. The films show gray and shiny appearance without visible adhesive failures upon ocular inspection. A typical cross-sectional SEM image is presented in Fig. 2 for a SiO_xN_y film deposited with a pulse frequency of 200 Hz and an N_2O flow of 10 sccm. The deposition rates scale with the frequency and pulse energy. Specifically, pulse energies of 3 and 6 J yielded 1.8 and 3.0 nm/s, respectively, while the deposition rate at 2 J was only 1.0 nm/s. According to $\theta/2\theta$ scans, the films are x-ray amorphous. Residual film stresses and densities did not show significant dependencies on the investigated parameters. The compressive stresses ranged between −650 and −960 MPa while a density of 2.45 ± 0.15 g/cm^3 was determined for all films. The obtained film densities are closer to that of a-Si (∼2.3 g/cm^3)[55] than to a-SiO_x (∼2.1 g/cm^3)[56] or a-SiN_x (∼3.0 g/cm^3),[57] which agrees with the silicon-rich atomic composition of the SiO_xN_y films (see next paragraph).

The atomic concentrations of oxygen and nitrogen in the films as obtained by ERDA are shown in Figs. 3(a)–3(c). The overall film oxygen and nitrogen content is influenced by the N_2O flow, while the film O/N-ratio is tuned with the pulse frequency and pulse energy. As shown in Fig. 3(a), the O and N content of the SiO_xN_y films increase as the N_2O flow increases. The O/N-ratio is not significantly affected by

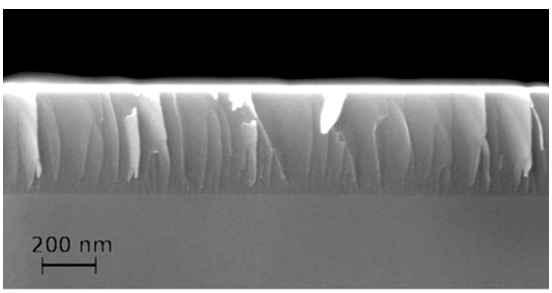

FIG. 2. Cross-sectional SEM image of a film deposited with pulse frequency of 200 Hz at N_2O flow of 10 sccm. Charging effects due to the insulating properties of the film are visible in the image.

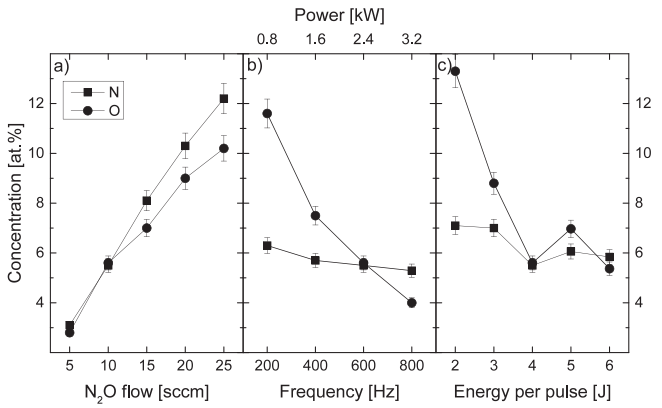

FIG. 3. Atomic concentrations of N and O in the films as obtained by ERDA, for the variation of (a) the N_2O flow rate, (b) the pulse frequency at a constant pulse energy of 4 J, and (c) the pulse energy at constant pulse frequency of 600 Hz.

the N_2O flow. In Fig. 3(b), the effect of increasing frequencies from 200 Hz to 800 Hz and average target powers from 0.8 to 3.2 kW on the film composition is shown. Here, a strong reduction of the O content by ∼8 at.% is observed, while the N content is hardly affected. The change in composition corresponds to O/N-ratios between ∼1.8 and ∼0.8. Figure 3(c) shows the O and N content with increasing pulse energies. Increasing the pulse energy from 2 to 6 J results in a decreased film O content from ∼13 to ∼5 at.%, while the N content does not show a strong dependence on the pulse energy. The decreasing O content results in a reduction of the film O/N-ratio from ∼1.9 to ∼0.9. In addition, ERDA reveals that the films contain argon (∼3 at.%) and trace amounts of carbon (≲0.1 at.%).

The oxygen surplus at low pulse frequencies and pulse energies is ascribed to a preferred formation of film forming O-containing precursor species. Low energies per pulse and low average target powers promote the creation of NO^+ and O^+, but not N^+ and N_2^+, since the oxygen-containing species show lower appearance energies (cf. Table II). The inherently high reactivity of oxygen, elevated sticking coefficient, as well as the higher electronegativity compared to nitrogen, also contributes to the surface reactions at the substrate and the target, leading to an oxygen surplus in the films.[51,58] At the same time, for the depositions using 10 sccm N_2O, changes regarding the peak target current were not observed when varying pulse frequencies while keeping the energy per pulse at 4 J. This suggests that the target surface is not affected noticeably by a lowered average power and increased pulse off-times during the depositions. The film oxygen surplus is most distinct when low pulse frequencies and thus extended pulse off-times or low pulse energies and thus reduced sputter rates are applied. Here, a higher percentage of the sputtered material is available for chemical reactions with reactive gaseous species at the substrate. The composition of the films is supposed to be mainly determined by reactions at the substrate surface as the ionization mean free path of the sputtered target material is estimated to be over twice as large as the target–substrate distance (60 mm).[59] This decreases the probability of gas-phase

reactions. In this context, it should be noted that the $f_{N_2O/Ar}$ was only 2.4% during depositions, reducing the probability for gas-phase reactions further.

The composition of SiON thin films deposited at pulse frequencies >500 Hz and energies >4 J is determined by the raised sputter rate of atomic Si. Consequently, the O and N contents in the films are reduced. Additionally, high energies per pulse lead to gas rarefaction in front of the target. Gas rarefaction lowers the collision probability of the sputtered material with the gaseous species further and yields even less amount of deposited compound material.[59] In contrast to the considerably reduced oxygen contents in the films, the nitrogen content is hardly affected by the change in energetics of the deposition process. According to appearance energies and energies for dissociative ionization (cf. Table II and dissociation reactions), the steady N content in the films at increased pulse energies is understood to be a consequence of the favored formation of N^+ and N_2^+.

The chemical bond structure of the SiON films was assessed by the evaluation of the XPS Si 2p core level spectra obtained from as-deposited samples. Due to the amorphous nature of the films, it can be assumed that Si is bond to Si, O, and N in a random manner. Contributing to this assumption is the fact that HiPIMS processes are far from thermal equilibrium,[19] supporting a random bond structure in the films.[60] As a consequence of the stochastic nature of the bond formation process and thus the lack of repeating unit cells, as well as the existence of nearest-neighbor effects, broad bond contributions of up to 1.6 eV in FWHM are observed. Due to the comparatively low O and N contents in the films, all O and N is bond to Si. This is also corroborated by corresponding N 1s and O 1s core level spectra, presenting one broad, featureless peak, indicating no O–N bonding in the films.

Figures 4–6 show the Si 2p core level spectra of the SiO_xN_y films deposited with varying N_2O flows, pulse frequencies, and pulse energies, respectively. Based on the information acquired from our reference samples, the Si 2p core level spectra were deconvoluted into five components, two for the characteristic Si 2p doublet (Si $2p_{3/2}$ at 98.85 ± 0.10 eV, Si $2p_{1/2}$ at 99.45 ± 0.10 eV), one component assigned to the Si–N bond at 99.90 ± 0.10 eV, another to the Si–O bond at 102.70 ± 0.10 eV, and an intermediate contribution at 101.10 ± 0.15 eV between the peaks referred as Si–O/N. This contribution is assigned to Si–N, which is affected by O as next neighbor. The SiO_xN_y deposited at $f_{N_2O/Ar}$ of 1.2% [Fig. 4(a)] is an exception with respect to the intermediate peak position as this peak is found at 101.60 eV. The deviation is attributed to surface oxide as this particular film presents the least O and N contents of all films. As the spectra were obtained from as-deposited samples, the relative increase of O at the surface contributes to a shift toward higher binding energies. Due to the amorphous nature of the films, the peaks assigned to O and N bond contributions are comparatively broad and thus set a limit to the accuracy of the peak fit model regarding the different bonding states in the films. The bonding configuration in amorphous SiO_xN_y films have been shown to be many fold, and

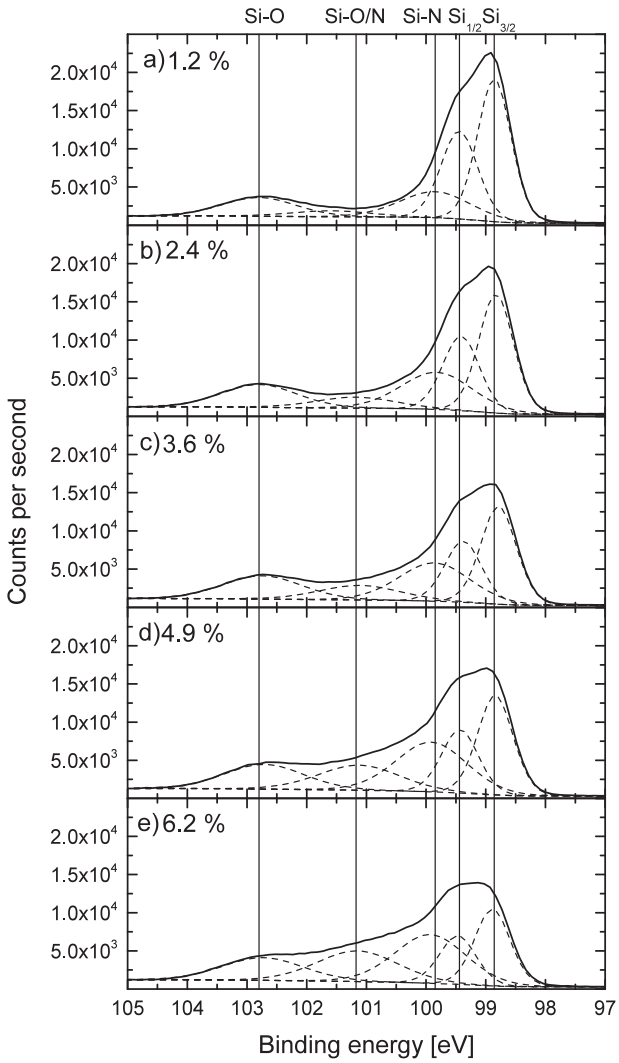

FIG. 4. XPS Si 2p core level spectra of the films deposited with different N_2O/Ar flow ratios. Flow ratios, core level components, as well as component positions are indicated.

the choice of applicable bond models depends also on the deposition temperature as well as on other parameters such as ion bombardment affecting film growth dynamics during deposition.[60,61]

The relative contributions of the three elements Si, N, and O to the total Si 2p area are shown in Fig. 7. For this purpose, the Si–O/N component was split between these two based on the O/N-ratio of the film. Increasing N_2O flows result in an increased number of Si–O and Si–N bonds, correlating with the increasing atomic concentrations of both elements [cf. Fig. 7(a)]. This relation is not as obvious for the frequency and pulse energy series; as the O/N-ratio in the films ranges between 1.9 and 0.8, the peak position of the intermediate peak is shifted toward lower binding energies with decreasing O/N-ratio, i.e., decreasing frequency or pulse energy (cf. Figs. 5 and 6). The shift of the contribution assigned to Si–O/N can be explained by reduced influence of O as the O/N-ratio decreases. A more detailed analysis of the bonding is not pursued, as our model contains only three components for Si–O/Si–N bonds.

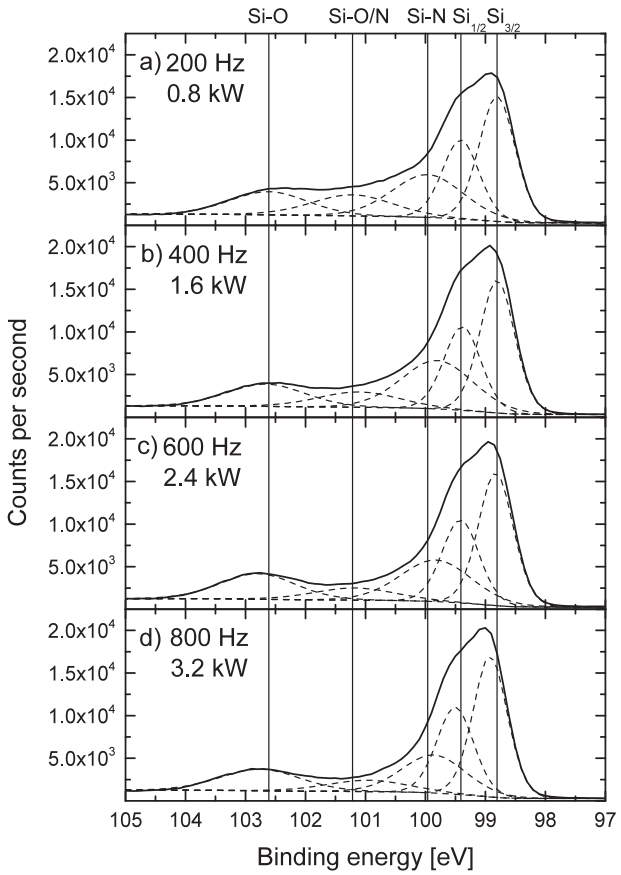

FIG. 5. XPS Si 2p core level spectra of the films deposited with different pulse frequencies. Frequencies, core level components, as well as component positions are indicated.

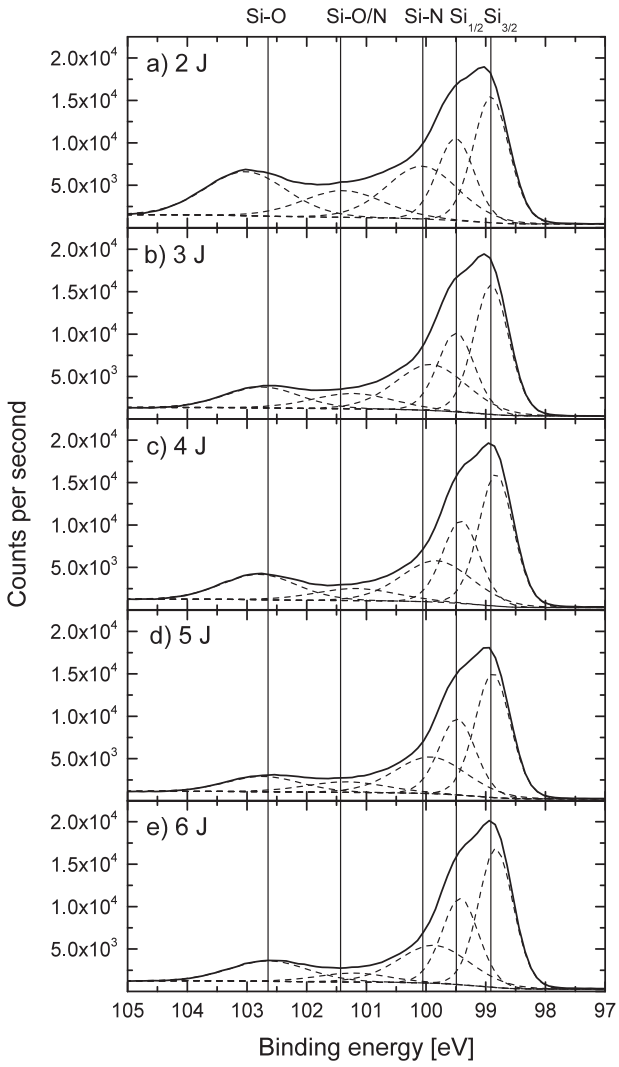

FIG. 6. XPS Si 2p core level spectra of the films deposited with different pulse energies. Pulse energies, core level components, as well as component positions are indicated.

C. Film optical properties

The optical properties of the films show a strong correlation to the percentage of both oxygen and nitrogen in the films. The film refractive indices n and extinction coefficients k were obtained from the Tauc–Lorentz model fitted to the ellipsometric data collected for each sample.[62] Refractive indices and extinction coefficients for all films at the wavelength of 633 nm are shown in Fig. 8. Refractive index values for amorphous Si (dashed line at $n = 4.5$), SiO_2 (dashed–dotted line at $n = 1.45$), and SiN_x (short dashed line at $n = 2.0$), as well as the extinction coefficient value of a-Si (dotted line at $k = 0.38$) are indicated as horizontal lines in the subfigures. Values of a-Si and SiO_2 were recorded for the reference samples used in XPS, n for SiN_x from Ref. 63.

As is shown in Figs. 8(a)–8(c), increased N_2O flow rates as well as decreased pulse frequencies and energies result in equivalent film optical properties. Both n and k follow the film elemental composition; increased total O and N contents yield lower values. The shape of the n and k dispersion curves remains the same due to comparable elemental composition and morphology of the films.[63] As the films are Si-rich the n and k values remain still closer to a-Si than to SiO_xN_y, i.e., the films have nonzero extinction coefficients and high refractive indices.[63] Due to the comparatively low film O and N concentrations the optical properties are

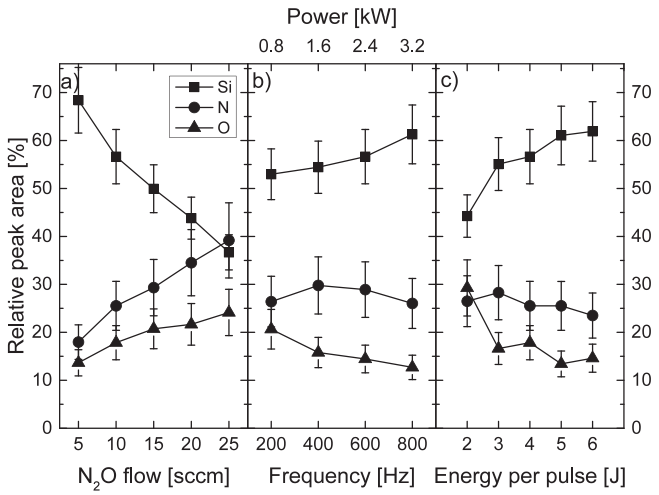

FIG. 7. Relative peak areas of the assigned contributions in the Si 2p core level spectra for films deposited in different (a) $f_{N_2O/Ar}$, (b) pulse frequencies, and (c) pulse energies.

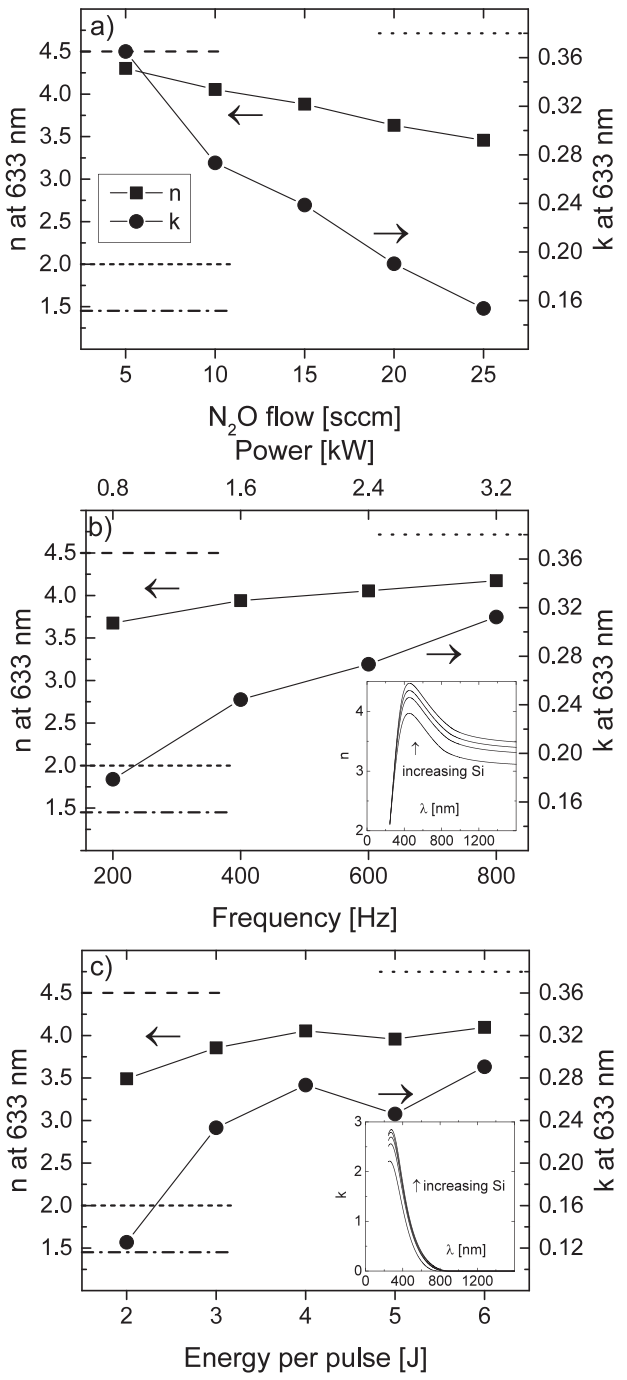

FIG. 8. Refractive indices n and extinction coefficient k for SiO_xN_y films deposited by variation of (a) the $f_{N_2O/Ar}$, (b) the pulse frequencies, and (c) the pulse energies. The refractive indices for a-Si (dashed line at $n = 4.5$), SiO_2 (dashed–dotted line at $n = 1.45$), and SiN_x (short dashed line at $n = 2.0$) as well as the extinction coefficient of a-Si (dotted line at $k = 0.38$) are indicated as horizontal lines in the subfigures. The inset of (b) shows the n-dispersion for films deposited with varying pulse frequencies whereas the inset of (c) shows the k-dispersion for films deposited with different average powers.

governed by the Si-rich nature of the films and the O/N-ratio does not have an observable effect on the n and k values.

IV. CONCLUSIONS

Silicon-rich silicon oxynitride films were synthesized by rHiPIMS at a constant process pressure of 400 mPa using different N_2O/Ar flow ratios. The amount of oxygen and nitrogen in the films can be controlled by adjusting the N_2O flow to affect the concentrations of both oxygen and nitrogen. The film O/N-ratio can be tuned in the range of 0.8–1.9 by changing the pulse frequency between 200 and 800 Hz while maintaining a pulse energy of 4 J, or by changing the energy per pulse between 2 and 6 J, with higher frequencies and pulse energies resulting in lower O/N-ratios. Under these deposition conditions, the films are amorphous and exhibit random chemical bonding. Optical properties of the films are governed by their Si-rich nature, resulting in refractive indices and extinction coefficients that are closer to a-Si values than to silicon oxynitride. The control of O/N-ratio by pulse frequency and energy poses pathways to tailor the film chemical composition from O-rich SiON to N-rich SiON.

ACKNOWLEDGMENTS

Roger Magnusson is gratefully acknowledged for assistance with the ellipsometry measurements. The authors acknowledge the funding by European Union's Seventh Framework Program (FP7/2007-2013) under the LifeLongJoints Project, Grant Agreement No. GA-310477. L.H. and H.H. acknowledge the Swedish Government Strategic Research Area in Materials Science on Functional Materials at Linköping University (Faculty Grant SFO-Mat-LiU No. 2009-00971) for financial support. The authors are thankful for access to the Tandem Laboratory at Uppsala University for ERDA measurements.

[1]T. S. Eriksson and C. G. Granqvist, J. Appl. Phys. **60**, 2081 (1986).
[2]M. Serényi, M. Rácz, and T. Lohner, Vacuum **61**, 245 (2001).
[3]H. Bartzsch, S. Lange, P. Frach, and K. Goedicke, Surf. Coat. Technol. **180–181**, 616 (2004).
[4]Y.-M. Xiong, P. G. Snyder, J. A. Woollam, G. Al-Jumaily, F. Gagliardi, and E. R. Krosche, Thin Solid Films **206**, 248 (1991).
[5]S. Callard, A. Gagnaire, and J. Joseph, Thin Solid Films **313–314**, 384 (1998).
[6]T. Kanata, H. Takakura, and Y. Hamakawa, Appl. Phys. A **49**, 305 (1989).
[7]D. V. Tsu, G. Lucovsky, M. J. Mantini, and S. S. Chao, J. Vac. Sci. Technol. A **5**, 1998 (1987).
[8]H. Kobayashi, T. Mizokuro, Y. Nakato, K. Yoneda, and Y. Todokoro, Appl. Phys. Lett. **71**, 1978 (1997).
[9]E. C. Samano, J. Camacho, and R. Machorro, J. Vac. Sci. Technol. A **23**, 1228 (2005).
[10]K. Worhoff, P. Lambeck, and A. Driessen, J. Lightwave Technol. **17**, 1401 (1999).
[11]B. S. Sahu, O. P. Agnihotri, S. C. Jain, R. Mertens, and I. Kato, Semicond. Sci. Technol. **15**, L11 (2000).
[12]E. Fogarassy, C. Fuchs, A. Slaoui, S. de Unamuno, J. P. Stoquert, W. Marine, and B. Lang, J. Appl. Phys. **76**, 2612 (1994).
[13]H. Fukuda, T. Arakawa, and S. Ohno, Jpn. J. Appl. Phys. **29**, L2333 (1990).
[14]K. Kumar, A. I. Chou, C. Lin, P. Choudhury, J. C. Lee, and J. K. Lowell, Appl. Phys. Lett. **70**, 384 (1997).
[15]N. Martin and C. Rousselot, J. Vac. Sci. Technol. A **17**, 2869 (1999).
[16]N. Martin, J. Lintymer, J. Gavoille, J. Chappé, F. Sthal, J. Takadoum, F. Vaz, and L. Rebouta, Surf. Coat. Technol. **201**, 7720 (2007).
[17]E. Aubry, S. Weber, A. Billard, and N. Martin, Appl. Surf. Sci. **257**, 10065 (2011).
[18]V. Kouznetsov, K. Macák, J. M. Schneider, U. Helmersson, and I. Petrov, Surf. Coat. Technol. **122**, 290 (1999).
[19]K. Sarakinos, J. Alami, and S. Konstantinidis, Surf. Coat. Technol. **204**, 1661 (2010).
[20]A. Ehiasarian, W.-D. Münz, L. Hultman, U. Helmersson, and I. Petrov, Surf. Coat. Technol. **163–164**, 267 (2003).

[21]I. Petrov, F. Adibi, J. E. Greene, L. Hultman, and J. Sundgren, Appl. Phys. Lett. **63**, 36 (1993).
[22]G. Håkansson, L. Hultman, J.-E. Sundgren, J. Greene, and W.-D. Münz, Surf. Coat. Technol. **48**, 51 (1991).
[23]G. Greczynski, J. Jensen, J. Böhlmark, and L. Hultman, Surf. Coat. Technol. **205**, 118 (2010).
[24]E. Wallin and U. Helmersson, Thin Solid Films **516**, 6398 (2008).
[25]K. Bobzin, N. Bagcivan, P. Immich, S. Bolz, R. Cremer, and T. Leyendecker, Thin Solid Films **517**, 1251 (2008).
[26]J. Alami, K. Sarakinos, F. Uslu, and M. Wuttig, J. Phys. D: Appl. Phys. **42**, 015304 (2009).
[27]P. Hovsepian, C. Reinhard, and A. Ehiasarian, Surf. Coat. Technol. **201**, 4105 (2006).
[28]S. Konstantinidis, J. Dauchot, and M. Hecq, Thin Solid Films **515**, 1182 (2006).
[29]S. Konstantinidis, A. Hemberg, J. P. Dauchot, and M. Hecq, J. Vac. Sci. Technol. B **25**, L19 (2007).
[30]H. Högberg, L. Tengdelius, M. Samuelsson, F. Eriksson, E. Broitman, J. Lu, J. Jensen, and L. Hultman, J. Vac. Sci. Technol. A **32**, 041510 (2014).
[31]M. Samuelsson, K. Sarakinos, H. Högberg, E. Lewin, U. Jansson, B. Wälivaara, H. Ljungcrantz, and U. Helmersson, Surf. Coat. Technol. **206**, 2396 (2012).
[32]S. Schmidt, G. Greczynski, C. Goyenola, G. Gueorguiev, Z. Czigány, J. Jensen, I. Ivanov, and L. Hultman, Surf. Coat. Technol. **206**, 646 (2011).
[33]D. W. Muenow, J. Chem. Phys. **60**, 3382 (1974).
[34]R. C. Wetzel, F. A. Baiocchi, T. R. Hayes, and R. S. Freund, Phys. Rev. A **35**, 559 (1987).
[35]D. W. Turner, Philos. Trans. R. Soc. London Ser. A **268**, 7 (1970).
[36]R. Rejoub, B. G. Lindsay, and R. F. Stebbings, Phys. Rev. A **65**, 042713 (2002).
[37]B. G. Lindsay, R. Rejoub, and R. F. Stebbings, J. Chem. Phys. **118**, 5894 (2003).
[38]J. Olivier, R. Locht, and J. Momigny, Chem. Phys. **68**, 201 (1982).
[39]J. Olivier, R. Locht, and J. Momigny, Chem. Phys. **84**, 295 (1984).
[40]F. Brüning, S. Matejcik, E. Illenberger, Y. Chu, G. Senn, D. Muigg, G. Denifl, and T. D. Märk, Chem. Phys. Lett. **292**, 177 (1998).
[41]M. Bowes and J. W. Bradley, J. Phys. D: Appl. Phys. **47**, 265202 (2014).
[42]P. J. Chantry, J. Chem. Phys. **51**, 3369 (1969).
[43]HiPIMS sputter coating system, see http://www.cemecon.de/coating_technology/coating_units/hipims_sputter_coating_system/index_eng.html.
[44]A. Rosakis, R. Singh, Y. Tsuji, E. Kolawa, and N. Moore, Jr., Thin Solid Films **325**, 42 (1998).
[45]G. Janssen, M. Abdalla, F. van Keulen, B. Pujada, and B. van Venrooy, Thin Solid Films **517**, 1858 (2009).
[46]H. J. Whitlow, G. Possnert, and C. Petersson, Nucl. Instrum. Methods Phys. Res. Sect. B **27**, 448 (1987).
[47]J. Jensen, D. Martin, A. Surpi, and T. Kubart, Nucl. Instrum. Methods Phys. Res. Sect. B **268**, 1893 (2010).
[48]D. J. Miller, M. C. Biesinger, and N. S. McIntyre, Surf. Interface Anal. **33**, 299 (2002).
[49]G. E. Jellison and F. A. Modine, Appl. Phys. Lett. **69**, 371 (1996).
[50]E. Hollands and D. Campbell, J. Mater. Sci. **3**, 544 (1968).
[51]D. Severin, O. Kappertz, T. Kubart, T. Nyberg, S. Berg, A. Pflug, M. Siemers, and M. Wuttig, Appl. Phys. Lett. **88**, 161504 (2006).
[52]A. Anders, Surf. Coat. Technol. **205**, S1 (2011).
[53]R. Baragiola, E. Alonso, J. Ferron, and A. Oliva-Florio, Surf. Sci. **90**, 240 (1979).
[54]A. Novikov, Solid-State Electron. **54**, 8 (2010).
[55]D. Lide, *CRC Handbook of Chemistry and Physics*, 95th ed. (Taylor & Francis, London, 2014).
[56]A. Bender, T. Gerber, H. Albrecht, and B. Himmel, Thin Solid Films **229**, 29 (1993).
[57]T. Serikawa and A. Okamoto, J. Electrochem. Soc. **131**, 2928 (1984).
[58]V. Gritsenko, R. Kwok, H. Wong, and J. Xu, J. Non-Cryst. Solids **297**, 96 (2002).
[59]*Reactive Sputter Deposition*, Springer Series in Materials Science, edited by D. Depla and S. Mahieu (Springer, Berlin, Heidelberg, 2008).
[60]P. Cova, S. Poulin, O. Grenier, and R. A. Masut, J. Appl. Phys. **97**, 073518 (2005).
[61]P. Cova, S. Poulin, and R. A. Masut, J. Appl. Phys. **98**, 094903 (2005).
[62]G. Jellison, Jr., F. Modine, P. Doshi, and A. Rohatgi, Thin Solid Films **313–314**, 193 (1998).
[63]Y.-N. Xu and W. Y. Ching, Phys. Rev. B **51**, 17379 (1995).